# Anapole-Plasmon Strong Coupling Induced Large Rabi Splitting in Dielectric-Metallic Hybrid Nanostructures

Wei Liu, Jinglei Wang, Haimei Luo, and Guiqiang Liu

***Abstract*—Manipulation of light-matter interaction is critical in modern physics, especially in the strong coupling regime. Based on the highly localized field enhancement in the near field, we demonstrate that strong coupling can be achieved in the dielectric-metallic hybrid structure consisting of a perforated Si nanoblock filled with a slotted Ag nanodisk (nanoprism) in its center. Large Rabi splitting of 275 (262) meV is achieved due to the generation of new hybrid energy states via the strong anapole-plasmon coupling. Our results pave a feasible way to realize large Rabi splitting and offer an attractive platform to explore strong coupling regime in the light-matter interaction.**

***Index Terms*—Light-matter interaction, strong coupling, rabi splitting.**

## I. Introduction

INTERACTION between light and matter has attracted considerable attention and has become the heart of modern optics due to its important role in optoelectronics, quantum optics and nanophotonic devices and so on [1], [2], [3]. Strong light-matter interaction might create new hybrid energy states with excellent application prospects in tunable low-threshold semiconductor lasers [4], low-energy switching [5] and cutting -edge nanophotonic devices, etc [6], [7], [8].

A specific regime of light-matter interaction can be realized when the intrinsic dissipation rate becomes slower than the rate of coherent energy exchange between matter and optical excitation [9]. Such a regime is called strong coupling, which can promote the formation of hybrid states of part-light and part-matter [10]. The half-light and half-matter bosonic quasi-particles are greatly important in quantum science, optoelectronics and nonlinear optics and so on [11], [12], [13], [14]. Strong coupling also opens up a lot of possibilities for fascinating advances such as Bose-Einstein condensation [15], [16], [17] and optical spin switching [18]. Therefore, manipulation of light-matter interaction in the strong coupling regime is critical in modern physics.

Exciton-polariton coupling in microcavities can serve as an excellent platform to control exciton conductance [19] and strong optical nonlinearity [20]. Initially, the observation of strong coupling was limited to experiments at cryogenic temperatures [21], [22], [23], [24]. With the development of nanoscience, various photonic and plasmonic nanostructures were used to achieve strong coupling at room temperature [25], [26], [27]. Hybridized states of part-light and part-matter characteristics formed in these structures were manifested by the mode splitting in the optical spectrum [22], [28]. As a result, two entirely hybrid energy states were produced, *i.e.*, Rabi splitting. This so-called Rabi splitting has a wide application range [29], including control and modification of chemical reactions [30], [31], [32], low-threshold lasers [33], optical switching [34] and quantum information processing [35].

Recently, strong coupling of plasmon-exciton, anapole- exciton, anapole-plasmon, and anapole-plasmon-exciton and the resulting Rabi splitting have drawing increasing attention [36], [37], [38], [39], [40], [41], [42], [43]. For example, strong plasmon-exciton coupling was realized in the hybrid structures of plasmonic nanostructures and two-dimensional (2D) transition-metal dichalcogenides and large Rabi splitting of 49.5−175 meV was achieved [37], [38], [39]. Strong anapole-exciton coupling was found in the Si nanodisk array with $WS_2$ in the center of nanodisks, resulting in large Rabi splitting of 151 meV [40]. Resonance coupling between molecular exciton and anapole took place in the Si nanodisk-molecular J-aggregate structure, leading to a large mode splitting of 161 meV [41]. Strong anapole-plasmon coupling in the Si nanodisk-Au nanostrip dimer system was also studied with Rabi splitting of 120 meV [42]. Moreover, coupling behaviors in the anapole-plasmon, anapole-exciton and anapole-plasmon-exciton systems were studied in the Si nanodisk-Ag nanodisk, Si nanodisk-$WSe_2$ and Si nanodisk-Ag nanodisk-$WSe_2$ heterostructures, respectively [43]. The hybrid coupling of anapole, plasmon and exciton exhibited small far field scattering and large near field enhancement and thus induced larger Rabi splitting of 159 meV than that obtained in the anapole-exciton (79.5 meV) and anapole-plasmon (145 meV) systems. Larger Rabi splitting has also been experimentally achieved in complex structures, e.g., Si nanoparticle-monolayer $WS_2$-Au film nanocavity (240

Manuscript received 13 April 2023; revised 24 July 2023; accepted 15 August 2023. Date of publication 21 August 2023; date of current version 25 August 2023. This work was supported in part by the National Natural Science Foundation of China (NSFC) under Grants 62275112 and 51761015 and in part by the Science and Technology Key Project of Education Department of Jiangxi Province under Grant GJJ2200306. *(Corresponding author: Guiqiang Liu.)*

The authors are with the College of Physics and Communication Electronics, Jiangxi Normal University, Nanchang, Jiangxi 330022, China (e-mail: 202140100607@jxnu.edu.cn; 202040100572@jxnu.edu.cn; jxsdhm@jxnu.edu.cn; liugq@jxnu.edu.cn).

Digital Object Identifier 10.1109/JPHOT.2023.3306745

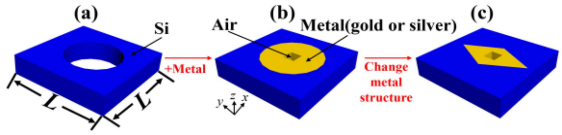


Fig. 1. Schematics of (a) perforated Si nanoblock, (b) Si nanoblock-metal nanodisk hybrid nanostructure and (c) Si nanoblock-metal nanoprism hybrid nanostructure.

meV) [44], Ag nanodisk array-monolayer $WS_2$-$MgF_2$-Ag film nanocavity (300 meV) [45] and Au@Ag nanorods-molecular J-aggregates (338 meV) [46]. These provide a new route for further exploiting strong coupling systems and mechanisms. However, the complicated fabrication process or relatively weak coupling strength hinders their further development.

In this work, we take an alternative route by utilizing the anapole modes in the cube nano-pixel geometry [47] to acquire large Rabi splitting. Strong coupling appears between the anapole and localized surface plasmon modes in the Si nanoblock-Ag nanodisk (nanoprism) hybrid structures and considerable Rabi splitting of 275 (262) meV is achieved. The obtained Rabi splitting in the Si nanoblock-Ag nanodisk (nanoprism) hybrid nanostructure is larger than those reported in Refs. [40], [41], [42], [43]. Our findings open new horizons to develop strong coupling effect for superior optoelectronic applications at nanoscales.

## II. Design and Method

Fig. 1 shows the schematics of the perforated Si nanoblock (a), the perforated Si nanoblock filled with the slotted metallic nanodisk (b) and nanoprism (c). The shape of perforation in the Si nanoblock corresponds to the shape of metal component in the hybrid structure. Au and Ag are employed to build the slotted nanodisk and nanoprism. The length and width of the air hole in the metal constituent both are 5 nm. The radius of Au or Ag nanodisk is 13 nm. The Au or Ag nanoprism is rhombus with the two diagonals of 50 nm and 140 nm. The heights of metallic nanodisk (nanoprism), Si nanoblock and air hole are all 50 nm. The length and width of the perforated Si nanoblock are the same and are denoted with $L$. A three- dimensional (3D) finite-difference time-domain (FDTD) method is used to execute the calculations. A total-field/scattered- field (TFSF) source with a wavelength ranging from 550 nm to 950 nm is used to act as the light source with the polarization along the $x$-axis direction. The permittivities of Si [48] and Au (Ag) [49] are taken from the published data. The mesh volume of Si nanoblock is $5 \times 5 \times 5$ nm$^3$. The mesh size is set to be 1 nm around the metallic constituent. The refractive index of surrounding medium is 1.0. Perfect matching layers are adopted in all directions.

## III. Results and Discussions

Fig. 2(a) presents the absorption cross-section spectra of the slotted Ag (black solid line) and Au nanodisks (black dashed line). Obvious absorption peaks indicate the excitation of localized surface plasmons. The scattering cross-section curves

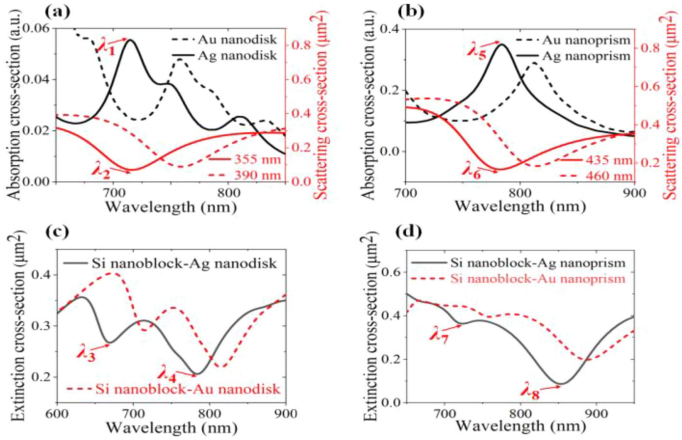


Fig. 2. Absorption and scattering cross-section curves of metal nanodisk and corresponding perforated Si nanoblock (a) and of metal nanoprism and corresponding perforated Si nanoblock (b). Extinction cross-section curves of Si nanoblock-metallic nanodisk (c) and Si nanoblock-metallic nanoprism hybrid nanostructures (d).

of corresponding perforated Si nanoblocks with $L = 355$ and 390 nm are also calculated and shown in Fig. 2(a), marked with red solid and dashed lines, respectively. Prominent scattering dips are observed here, indicating the excitation of anapole modes of perforated Si nanoblocks. The red-shift of scattering dip with $L$ indicates the tunable anapole mode. Moreover, the scattering dip at 715 nm of the perforated Si nanoblock with $L =$ 355 nm overlaps with that of the absorption peak of the slotted Ag nanodisk. For the perforated Si nanoblock with $L = 390$ nm, the scattering dip at 758 nm overlaps with that of the slotted Au nanodisk. The overlapping of the scattering dip of perforated Si nanoblock with the absorption peak of slotted metallic nanodisk, contributing to strong couple of localized surface plasmon and anapole when these two components are integrated together. Similar phenomena are found in the metal nanoprisms and corresponding perforated Si nanoblocks (Fig. 2(b)). As $L$ increases from 435 to 460 nm, the scattering dip of perforated Si nanoblock firstly overlaps with the absorption peak of Ag nanoprism and then with that of Au nanoprism.

To obtain the correct Rabi splitting, extinction cross-section curves of these two kinds of hybrid nanostructures were calculated [36]. Fig. 2(c) shows the extinction cross-section curves of the integrated Si nanoblock-Au (Ag) nanodisk hybrid nanostructures. Different from the only one dip found in the scattering cross-section curve of the perforated Si nanoblock and only one peak in the absorption spectrum of slotted metal nanodisk, there are two identifiable dips, denoted as the upper ($\lambda_3 = 668$ nm) and lower ($\lambda_4 = 784$ nm) hybrid energy modes, appearing in the Si nanoblock-metal nanodisk hybrid nanostructure. The lower and upper hybrid energy modes represent an anti-crossing behavior, indicating the resonance coupling effect of anapole and plasmon and large Rabi splitting [50], [51]. The two dips both shift to the longer wavelength region (corresponding 714 nm and 814 nm) when the Ag nanodisk is replaced by the Au nanodisk in the hybrid nanostructure. This again indicates the lower and upper hybrid energy modes derivation from the resonance

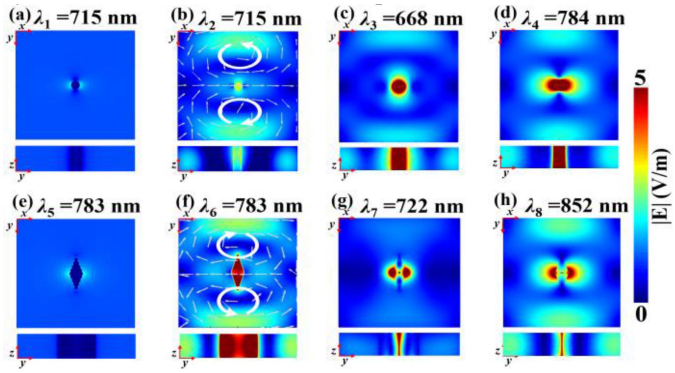


Fig. 3. (a)–(d) Electric field distributions in the *x*-*y* and *y*-*z* planes of slotted Ag nanodisk at $\lambda_1$, perforated Si nanoblock at $\lambda_2$ and Si nanoblock-Ag nanodisk hybrid structure at $\lambda_3$ and $\lambda_4$. (e)–(h) Electric field distributions in the *x*-*y* and *y*-*z* planes of slotted Ag nanoprism at $\lambda_5$, perforated Si nanoblock at $\lambda_6$ and Si nanoblock-Ag nanoprism hybrid structure at $\lambda_7$ and $\lambda_8$. Arrows: Direction of electric field energy flow.

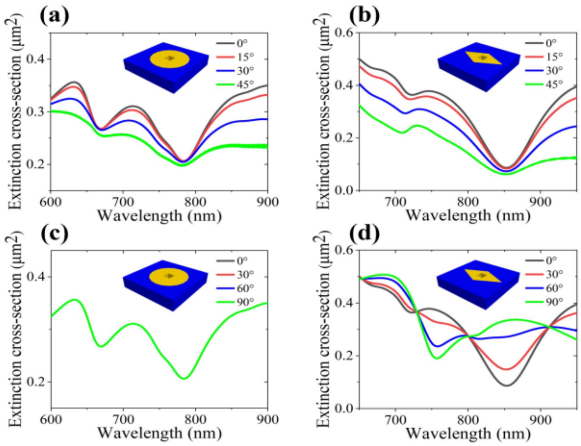


Fig. 4. Extinction cross-section curves of Si nanoblock-Ag nanodisk (a), (c) and Si nanoblock-Ag nanoprism hybrid nanostructures (b), (d) at different incident (a), (b) and polarization angles (c), (d).

coupling of plasmon and anapole. Moreover, the two dips both become shallow when the Ag nanodisk is replaced by the Au nanodisk with a decreased interval ($\Delta\lambda$ changing from 119 nm to 100 nm), indicating that larger Rabi splitting might be acquired in the hybrid nanostructure with Ag nanodisk. This can be explained by the fact that the resonance energy of Au nanodisk is larger but its coupling strength is lower than that of Ag nanodisk [52], [53].

When the slotted metallic nanoprism is inserted in the perforated Si nanoblock, similar phenomena are also observed in the extinction cross-section curves (Fig. 2(d)). The upper and lower hybrid energy modes both shift to the longer wavelength region with the increased *L*. Moreover, the dip in the short wavelength region is shallower than that observed in Fig. 2(c). While for the dip in the longer wavelength region, opposite phenomenon is obtained. These differences can be ascribed to the shape change of metal constituent in the hybrid structures. Moreover, for the hybrid nanostructure with a Ag nanoprism, the interval between the two distinct dips $\lambda_7$ (722 nm) and $\lambda_8$ (852 nm) is close to that obtained in the hybrid nanostructure with the Au nanoprism but the depths of these two dips both become shallower, again indicating the weakened coupling strength in the hybrid nanostructure with the Au nanoprism.

To understand the physical mechanisms of the phenomena observed in Fig. 2, corresponding electric field distributions in the *x*-*y* and *y*-*z* planes are calculated. Considering the similar optical properties of Au and Ag constituents with the same configurations, only the electric field distributions of the structures with Ag components are shown in Fig. 3. The electric field distribution pattern of the Ag nanodisk at $\lambda_1 = 715$ nm (Fig. 3(a)) verifies the excitation of localized surface plasmon. The electric field distribution and electric field energy flow directions of the perforated Si nanoblock at $\lambda_2 = 715$ nm (Fig. 3(b)) demonstrate the excitation of anapole mode in such a structure [41], [54], [55]. When the slotted Ag nanodisk is placed in the perforated Si nanoblock, the electric field energies for the dips at $\lambda_3 = 668$ nm and $\lambda_4 = 784$ nm both are mainly gathered in the center as shown in Fig. 3(c) and (d). These indicate the excitation of stronger localized surface plasmons of the Ag nanodisk. Strong electric energies in the neighborhoods, with similar distribution patterns to that of the perforated Si nanoblock, are also observed here, implying the excitation of anapole mode simultaneously. That is, strong coupling of anapole and plasmon occurs and then promotes the appearance of the upper and lower energy modes in such hybrid nanostructures. Moreover, the energies of these two dips both are stronger than those observed in Fig. 3(a) and (b), demonstrating that the anapole mode can enhance the light-matter interaction via the strong coupling effect.

Fig. 3(e)–(h) displays the electric field distributions for the slotted Ag nanoprism, perforated Si nanoblock and their integrated structure at resonance modes, respectively. Similar electric field distribution patterns again verify the excited localized surface plasmon of Ag nanoprism, anapole of perforated Si nanoblock and strong coupling of anapole and plasmon in the integrated structure at $\lambda_7 = 722$ nm and $\lambda_8 = 852$ nm. For the dip at $\lambda_7 = 722$ nm, although the coupling of anapole and plasmon can also be found here, the surrounding electric field energy is very weaker than that in the center, implying the domination role of localized surface plasmon on this dip. This might be attributed to the particular shape of Ag nanoprism with two unequal diagonals. These findings again imply that the Rabi splitting can be ascribed to the excited plasmon and anapole modes and their strong resonance couple effect.

Angle-resolved extinction cross-section spectra of Si nanoblock- Ag nanodisk and Si nanoblock-Ag nanoprism hybrid nanostructures are shown in Fig. 4(a) and (b), respectively. It can be clearly seen that the positions of the two dips in these two structures are almost invariable but the depths both become shallow and shallow when the incident angle increases from 0, 15, 30, and 45° in intervals of 15°. These illustrate that the incidence angle effect on the Rabi splitting can be ignored when it is less than 45°.

Fig. 4(c) and (d) respectively shows the extinction cross-section curves of Si nanoblock-Ag nanodisk and Si nanoblock-Ag nanoprism nanostructures at different polarization angles. No distinct change can be found in the curve of the Si nanoblock-

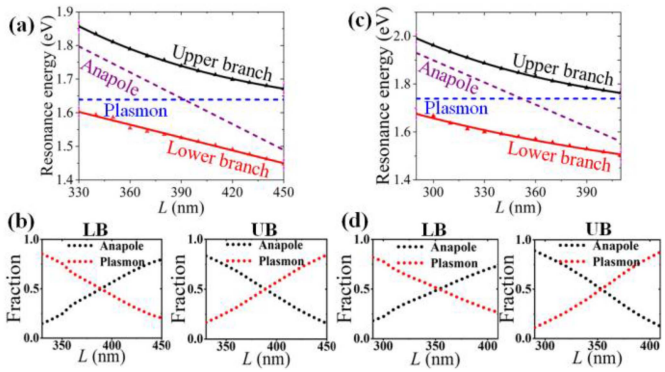


Fig. 5. Dispersion curves of (a) Si nanoblock-Au nanodisk. (b) Hopfield coefficients for anapole and plasmon contributions to UB and LB. Si nanoblock-Ag nanodisk hybrid nanostructures. Dispersion curves of (c) Si nanoblock-Ag nanodisk. (d) Hopfield coefficients for anapole and plasmon contributions to UB and LB.

Ag nanodisk hybrid nanostructure with the polarization angle increasing from 0 to 90° with a step of 30° (from TM to TE polarization), indicating the polarization-insensitivity of Rabi splitting. Differentially, opposite change trends in depths and positions of these two dips in the Si nanoblock-Ag nanoprism hybrid nanostructure imply the polarization-dependence of Rabi splitting, which can be ascribed to the specific shape of Ag nanorpism with unequal diagonals.

In order to identify the anapole-plasmon coupling behavior, dispersion curves of perforated Si nanoblock, slotted Au nanodisk and their hybrid nanostructure are calculated by changing the $L$ of the perforated Si nanoblock. The results are depicted in Fig. 5(a). An obvious anti-crossing behavior is exhibited in the energy of the lower branch (LB) and upper branch (UB), ensuring the Rabi splitting. When the energies of the uncoupled plasmon mode ($E_{\mathrm{P}}$) and anapole mode ($E_{\mathrm{A}}$) are equal (zero detuning, $\delta = E_{\mathrm{P}} - E_{\mathrm{A}} = 0$), large Rabi splitting can be extracted as the minimal splitting occurs between the LB and UB [3], [53]. Hopfield coefficients of UB and LB that illustrate the intermixing behavior between the anapole and plasmon are displayed in Fig. 5(b). The contribution of uncoupled states in the hybrid structure can be obtained via the energy fraction of plasmon and anapole [53], [56]. The large Rabi splitting $\hbar\Omega$, proportional to the coupling strength $g$ ($\hbar\Omega = 2$ g) [40], [41], [42], [43], [53], can be obtained as $\delta = 0$. Here, it can easily obtain that the Rabi splitting value is $\hbar\Omega_{\mathrm{AP}} = 214$ meV when $L = 390$ nm, satisfying the strong coupling criterion [57], [58]: $\hbar\Omega_{\mathrm{AP}} > (\hbar\Gamma_{\mathrm{A}} + \hbar\Gamma_{\mathrm{p}})/2$ between the plasmon ($\hbar\Gamma_{\mathrm{p}} = 169$ meV) and anapole ($\hbar\Gamma_{\mathrm{A}} = 179$ meV) modes. Negative detuning ($\delta < 0$) implies a larger anapole fraction in UB and smaller anapole fraction in LB. Positive detuning ($\delta > 0$) indicates a larger plasmon fraction in UB and smaller plasmon fraction in LB. In this work, the detuning is modulated by the anapole mode to obtain larger Rabi splitting with $\delta = 0$.

When the Au nanodisk is replaced by the Ag nanodisk, corresponding dispersion curves and Hopfield coefficients for anapole and plasmon contributions to UB and LB are shown in Fig. 5(c) and (d), respectively. The calculated Rabi splitting is as high as 275 meV when $L = 355$ nm, larger than that of the Si nanoblock-Au nanodisk nanostructure. Large Rabi splitting of 262 meV can also be achieved in the Si nanodisk-Ag nanoprism hybrid nanostructure with $L = 435$ nm, also larger than 240 meV obtained in the Si nanodisk-Au nanoprism hybrid nanostructure with $L = 460$ nm. These results again demonstrate the appearance of strong anapole-plasmon hybrid energy states and superior Rabi splitting in such structures.

TABLE I
COUPLING RELATED TO NANOSTRUCTURE LITERATURE COMPARISON

| Ref. | Hybrid structure | Coupling type | Rabi splitting (meV) |
|---|---|---|---|
| [40] | Si nanodisk-bulk $WS_2$ | anapole-exciton | 151 (cal.) |
| [41] | Si nanodisk-molecular J-aggregates ring | anapole-exciton | 161 (cal.) |
| [42] | Si nanodisk-Au nanostrip dimer | anapole-plasmon | 120 (cal.) |
| [43] | Si nanodisk-Ag nanodisk | anapole-plasmon | 145 (cal.) |
| [43] | Si nanodisk-monolayer $WSe_2$ | anapole-exciton | 79.5 (cal.) |
| [43] | Si nanodisk-Ag nanodisk-monolayer $WSe_2$ | anapole-plasmon-exciton | 159 (cal.) |
| [44] | Si nanoparticle-monolayer $WS_2$-Au film nanocavity | plasmon-MMD (mirror-image-induced magnetic dipole)-exciton | 240 (exp.) |
| [45] | Ag nanodisk array-monolayer $WS_2$-$MgF_2$-Ag film nanocavity | plasmon-exciton | 300 (exp.) |
| [46] | Au@Ag nanorods-molecular J aggregates | plasmon-exciton | 338 (exp.) |
| [50] | Au nanohole-monolayer $WS_2$ | plasmon-exciton | 162 (exp.) |
| Our work | Si nanoblock-Ag nanodisk (nanoprism) | anapole-plasmon | 275 (262) (cal.) |

Table I shows a brief comparison of coupling related nanostructures and Rabi splitting values in previous works (including calculation (cal.) and experiment (exp.)) and our work. Obviously, our proposed nanostructures are with the Rabi splitting value larger than those observed in the conventional nanostructures [40], [41], [42], [43], [50] and are simpler than those with close Rabi splitting values reported in Refs. [44], [45], [46]. Our findings open a new way for realizing strong anapole-plasmon coupling and large Rabi splitting in simple nanostructures.

## IV. CONCLUSION

In summary, we have successfully demonstrated that strong coupling between the anapole and plasmon modes can be realized in the Si nanoblock-Au (Ag) nanodisk (nanoprism) hybrid structures. Two anapole-plasmon hybrid states are generated in such structures. Large Rabi splitting value reaching to 275 meV is achieved when the slotted Ag nanodisk is inserted in the perforated Si nanoblock, larger than those obtained in the anapole-plasmon systems reported previously [41], [42]. Furthermore, these hybrid nanostructures are simpler than those reported in Refs. [44], [45], [46]. Our findings open a new way to realize strong coupling of anapole-plasmon and pave an excellent platform to manipulate the light-matter interaction in optoelectronic field at nanoscales.

## REFERENCES


[1] G. Eda and S. A. Maier, "Two-dimensional crystals: Managing light for optoelectronics," *Amer. Chem. Soc. Nano*, vol. 7, no. 7, pp. 5660–5665, Jul. 2013.

[2] F. Monticone and A. Alu, "Metamaterial, plasmonic and nanophotonic devices," *Rep. Prog. Phys.*, vol. 80, no. 3, Feb. 2017, Art. no. 036401.

[3] Y. Lu et al., "Cylindrical vector beams reveal radiationless anapole condition in a resonant state," *Opto-Electron. Adv.*, vol. 5, no. 4, Feb. 2022, Art. no. 210014.

[4] S. Christopoulos et al., "Room-temperature polariton lasing in semiconductor microcavities," *Phys. Rev. Lett.*, vol. 98, no. 12, Mar. 2007, Art. no. 126405.

[5] A. Dreismann et al., "A sub-femtojoule electrical spin-switch based on optically trapped polariton condensates," *Nature Mater.*, vol. 15, no. 10, pp. 1074–1078, Oct. 2016.

[6] F. Deng, H. Liu, L. Xu, S. Lan, and A. E. Miroshnichenko, "Strong exciton-plasmon coupling in a $WS_2$ monolayer on Au film hybrid structures mediated by liquid Ga nanoparticles," *Laser Photon. Rev.*, vol. 14, no. 4, Apr. 2020, Art. no. 1900420.

[7] Y. Jiang, H. Wang, S. Wen, H. Chen, and S. Deng, "Resonance coupling in an individual gold nanorod-monolayer WS2 heterostructure: Photoluminescence enhancement with spectral broadening," *Amer. Chem. Soc. Nano*, vol. 14, no. 10, pp. 13841–13851, Oct. 2020.

[8] S. Wang et al., "Coherent coupling of $WS_2$ monolayers with metallic photonic nanostructures at room temperature," *Nano Lett.*, vol. 16, no. 7, pp. 4368–4374, Jul. 2016.

[9] P. Vasa and C. Lienau, "Strong light-matter interaction in quantum emitter/metal hybrid nanostructures," *Amer. Chem. Soc. Photon.*, vol. 5, no. 1, pp. 2–23, Jan. 2018.

[10] J. Flick, N. Rivera, and P. Narang, "Strong light-matter coupling in quantum chemistry and quantum photonics," *Nanophotonics*, vol. 7, no. 9, pp. 1479–1501, Sep. 2018.

[11] C. Monroe, "Quantum information processing with atoms and photons," *Nature*, vol. 416, no. 6877, pp. 238–246, Mar. 2002.

[12] D. E. Chang, A. S. Sørensen, E. A. Demler, and M. D. Lukin, "A single-photon transistor using nanoscale surface plasmons," *Nature Phys.*, vol. 3, no. 11, pp. 807–812, Nov. 2007.

[13] P. Bhattacharya, T. Frost, S. Deshpande, M. Z. Baten, A. Hazari, and A. Das, "Room temperature electrically injected polariton laser," *Phys. Rev. Lett.*, vol. 112, no. 23, Jun. 2014, Art. no. 236802.

[14] T. Shibanuma, G. Grinblat, P. Albella, and S. A. Maier, "Efficient third harmonic generation from metal-dielectric hybrid nanoantennas," *Nano Lett.*, vol. 17, no. 4, pp. 2647–2651, Apr. 2017.

[15] J. Kasprzak et al., "Bose–Einstein condensation of exciton polaritons," *Nature*, vol. 443, no. 7110, pp. 409–414, Sep. 2006.

[16] H. Deng, H. Haug, and Y. Yamamoto, "Exciton-polariton bose-einstein condensation," *Rev. Modern Phys.*, vol. 82, no. 2, pp. 1489–1537, May 2010.

[17] J. D. Plumhof, T. Stoeferle, L. Mai, U. Scherf, and R. F. Mahrt, "Room-temperature Bose–Einstein condensation of cavity exciton-polaritons in a polymer," *Nature Mater.*, vol. 13, no. 3, pp. 248–253, Mar. 2014.

[18] A. Amo et al., "Exciton-polariton spin switches," *Nature Photon.*, vol. 4, no. 6, pp. 361–366, Apr. 2010.

[19] J. Feist and F. J. Garcia-Vidal, "Extraordinary exciton conductance induced by strong coupling," *Phys. Rev. Lett.*, vol. 114, no. 19, May 2015, Art. no. 196402.

[20] G. Khitrova, H. Gibbs, F. Jahnke, M. Kira, and S. Koch, "Nonlinear optics of normal-mode-coupling semiconductor microcavities," *Rev. Modern Phys.*, vol. 71, no. 5, pp. 1591–1639, Oct. 1999.

[21] J. P. Reithmaier et al., "Strong coupling in a single quantum dot-semiconductor microcavity system," *Nature*, vol. 432, no. 7014, pp. 197–200, Nov. 2004.

[22] T. Yoshie et al., "Vacuum Rabi splitting with a single quantum dot in a photonic crystal nanocavity," *Nature*, vol. 432, no. 7014, pp. 200–203, Nov. 2004.

[23] F. Milde, A. Knorr, and S. Hughes, "Role of electron-phonon scattering on the vacuum Rabi splitting of a single-quantum dot and a photonic crystal nanocavity," *Phys. Rev. B*, vol. 78, no. 3, Jul. 2008, Art. no. 035330.

[24] E. Peter et al., "Exciton-photon strong-coupling regime for a single quantum dot embedded in a microcavity," *Phys. Rev. Lett.*, vol. 95, no. 6, Aug. 2005, Art. no. 067401.

[25] F. Stete, W. Koopman, and M. Bargheer, "Signatures of strong coupling on nanoparticles: Revealing absorption anticrossing by tuning the dielectric environment," *Amer. Chem. Soc. Photon.*, vol. 4, no. 7, pp. 1669–1676, Jul. 2017.

[26] T. J. Antosiewicz, S. P. Apell, and T. Shegai, "Plasmon-exciton interactions in a core-shell geometry: From enhanced absorption to strong coupling," *Amer. Chem. Soc. Photon.*, vol. 1, no. 5, pp. 454–463, May 2014.

[27] L. Zhang, R. Gogna, W. Burg, E. Tutuc, and H. Deng, "Photonic-crystal exciton-polaritons in monolayer semiconductors," *Nature Commun.*, vol. 9, no. 1, Feb. 2018, Art. no. 713.

[28] A. F. Koenderink, A. Alu, and A. Polman, "Nanophotonics: Shrinking light-based technology," *Science*, vol. 348, no. 6234, pp. 516–521, May 2015.

[29] E. Cao, W. Lin, M. Sun, W. Liang, and Y. Song, "Exciton-plasmon coupling interactions: From principle to applications," *Nanophotonics*, vol. 7, no. 1, pp. 145–167, Jan. 2018.

[30] A. Thomas et al., "Ground-state chemical reactivity under vibrational coupling to the vacuum electromagnetic field," *Angewandte Chemie-Int. Ed.*, vol. 55, no. 38, pp. 11462–11466, Sep. 2016.

[31] J. Lawless, C. Hrelescu, C. Elliott, L. Peters, N. McEvoy, and A. L. Bradley, "Influence of gold nano-bipyramid dimensions on strong coupling with excitons of monolayer $MoS_2$," *Amer. Chem. Soc. Appl. Mater. Interfaces*, vol. 12, no. 41, pp. 46406–46415, Oct. 2020.

[32] A. Thomas et al., "Ground state chemistry under vibrational strong coupling: Dependence of thermodynamic parameters on the Rabi splitting energy," *Nanophotonics*, vol. 9, no. 2, pp. 249–255, Feb. 2020.

[33] S. Noda, M. Fujita, and T. Asano, "Spontaneous-emission control by photonic crystals and nanocavities," *Nature Photon.*, vol. 1, no. 8, pp. 449–458, Aug. 2007.

[34] P. Vasa et al., "Ultrafast manipulation of strong coupling in metal-molecular aggregate hybrid nanostructures," *Amer. Chem. Soc. Nano*, vol. 4, no. 12, pp. 7559–7565, Dec. 2010.

[35] A. Imamog et al., "Quantum information processing using quantum dot spins and cavity QED," *Phys. Rev. Lett.*, vol. 83, no. 20, pp. 4204–4207, Nov. 1999.

[36] R. Du, H. Hu, T. Fu, Z. Shi, S. Zhang, and H. Xu, "How to obtain the correct Rabi splitting in a subwavelength interacting system," *Nano Lett.*, vol. 23, no. 2, pp. 444–450, Jan. 2023.

[37] D. Zheng, S. Zhang, Q. Deng, M. Kang, P. Nordlander, and H. Xu, "Manipulating coherent plasmon-exciton interaction in a single silver nanorod on monolayer $WSe_2$," *Nano Lett.*, vol. 17, no. 6, pp. 3809–3814, Jun. 2017.

[38] J. Cuadra, D. G. Baranov, M. Wersall, R. Verre, T. J. Antosiewicz, and T. Shegai, "Observation of tunable charged exciton polaritons in hybrid monolayer $WS_2$-plasmonic nanoantenna system," *Nano Lett.*, vol. 18, no. 3, pp. 1777–1785, Mar. 2018.

[39] M. Geisler et al., "Single-crystalline gold nanodisks on $WS_2$ mono- and multilayers for strong coupling at room temperature," *Amer. Chem. Soc. Photon.*, vol. 6, no. 4, pp. 994–1001, Apr. 2019.

[40] J. Wang, W. Yang, G. Sun, Y. He, P. Ren, and Z. Yang, "Boosting anapole-exciton strong coupling in all-dielectric heterostructures," *Photon. Res.*, vol. 10, no. 7, pp. 1744–1753, Jul. 2022.

[41] S.-D. Liu, J.-L. Fan, W.-J. Wang, J.-D. Chen, and Z.-H. Chen, "Resonance coupling between molecular excitons and nonradiating anapole modes in silicon nanodisk-J-aggregate heterostructures," *Amer. Chem. Soc. Photon.*, vol. 5, no. 4, pp. 1628–1639, Apr. 2018.

[42] K. Du et al., "Strong coupling between dark plasmon and anapole modes," *J. Phys. Chem. Lett.*, vol. 10, no. 16, pp. 4699–4705, Aug. 2019.

[43] K. As'ham, I. Al-Ani, L. Huang, A. E. Miroshnichenko, and H. T. Hattori, "Boosting strong coupling in a hybrid $WSe_2$ monolayer- anapole-plasmon system," *Amer. Chem. Soc. Photon.*, vol. 8, no. 2, pp. 489–496, Feb. 2021.

[44] F. Deng et al., "Greatly enhanced plasmon-exciton coupling in Si/$WS_2$/Au nanocavities," *Nano Lett.*, vol. 22, no. 1, pp. 220–228, Jan. 2022.

[45] B. Li et al., "Large Rabi splitting obtained in Ag-$WS_2$ strong-coupling heterostructure with optical microcavity at room temperature," *Opto-Electron. Adv.*, vol. 2, no. 5, May 2019, Art. no. 190008.

[46] D. Melnikau et al., "Double Rabi splitting in a strongly coupled system of core-shell Au@Ag nanorods and J-aggregates of multiple fluorophores," *J. Phys. Chem. Lett.*, vol. 10, no. 20, pp. 6137–6143, Oct. 2019.

[47] R. Wang and L. Dal Negro, "Engineering non-radiative anapole modes for broadband absorption enhancement of light," *Opt. Exp.*, vol. 24, no. 17, pp. 19048–19062, Aug. 2016.

[48] D. Edwards, Ed., *Handbook of Optical Constants of Solids*. New York, NY, USA: Academic, 1985.

[49] P. B. Johnson and R.-W. Christy, "Optical constants of the noble metals," *Phys. Rev. B*, vol. 6, no. 12, pp. 4370–4379, Dec. 1972.

[50] X. Chen, H. Wang, N.-S. Xu, H. Chen, and S. Deng, "Resonance coupling in hybrid gold nanohole-monolayer $WS_2$ nanostructures," *Appl. Mater. Today*, vol. 15, pp. 145–152, Jun. 2019.

[51] J. Wen, H. Wang, H. Chen, S. Deng, and N. Xu, "Room- temperature strong coupling between dipolar plasmon resonance in single gold nanorod and two-dimensional excitons in monolayer $WSe_2$," *Chin. Phys. B*, vol. 27, no. 9, Sep. 2018, Art. no. 096101.

[52] A. Cacciola, O. Di Stefano, R. Stassi, R. Saija, and S. Savasta, "Ultrastrong coupling of plasmons and excitons in a nanoshell," *Amer. Chem. Soc. Nano*, vol. 8, no. 11, pp. 11483–11492, Nov. 2014.

[53] J. Sun et al., "Light-emitting plexciton: Exploiting plasmon-exciton interaction in the intermediate coupling regime," *Amer. Chem. Soc. Nano*, vol. 12, no. 10, pp. 10393–10402, Oct. 2018.

[54] A. E. Miroshnichenko et al., "Nonradiating anapole modes in dielectric nanoparticles," *Nature Commun.*, vol. 6, no. 1, Aug. 2015, Art. no. 8069.

[55] B. Luk'yanchuk, R. Paniagua-Dominguez, A. I. Kuznetsov, A. E. Miroshnichenko, and Y. S. Kivshar, "Hybrid anapole modes of high-index dielectric nanoparticles," *Phys. Rev. A*, vol. 95, no. 6, Jun. 2017, Art. no. 063820.

[56] P. Jiang, G. Song, Y. Wang, C. Li, L. Wang, and L. Yu, "Tunable strong exciton–plasmon–exciton coupling in WS2-J-aggregates-plasmonic nanocavity," *Opt. Exp.*, vol. 27, no. 12, pp. 16613–16623, Jun. 2019.

[57] A. E. Schlather, N. Large, A. S. Urban, P. Nordlander, and N. J. Halas, "Near-field mediated plexcitonic coupling and giant Rabi splitting in individual metallic dimers," *Nano Lett.*, vol. 13, no. 7, pp. 3281–3286, Jul. 2013.

[58] G. Zengin, M. Wersäll, S. Nilsson, T. J. Antosiewicz, M. Käll, and T. Shegai, "Realizing strong light-matter interactions between single-nanoparticle plasmons and molecular excitons at ambient conditions," *Phys. Rev. Lett.*, vol. 114, no. 15, Apr. 2015, Art. no. 157401.